

Solvent-Free Process for Preparing Metal-Organic Framework Composites Based on Carbon-Based Quantum Dots and Their Derivatives as Drug Delivery Systems for Andrographolide

Wenndy Pantoja-Romero,^[a, b] Alexis Lavín-Flores,^[a, b] Gerardo Morell,^[b, c] Magaly Martínez-Ferrer,^[d, e] Brad R. Weiner,^[a, b] and Joaquín Coronas^{*[f, g]}

Andrographolide (ADG) was conjugated with MIL-53(Al), ZIF-8, carbon-based quantum dots (CBQDs) and doped carbon-based quantum dots (D-CBQDs) using high-pressure (0.3 GPa) contact. This solvent-free approach is environmentally friendly, energy-efficient, and time-saving, resulting in ADG-MOFs-CBQDs/D-CBQDs with physical properties comparable to those produced by traditional liquid phase encapsulation. The resulting nanocomposites were characterized using SEM, XRD, TGA, FT-IR, and ¹H NMR. The results indicate that ADG was partly encapsulated within the metal-organic framework (MOF) pores,

while another portion was bound externally to CBQD/D-CBQDs, as evidenced by distinct drug signals in each analysis. This green synthesis approach simplifies the conjugation process. It significantly enhances the drug solubility, as indicated by changes in hydrophobicity observed via ¹H NMR, surpassing the improvements achieved by ADG encapsulation within MOFs alone. Additionally, in preliminary tests, the materials exhibited significant cytotoxicity against PC3 cells compared to ADG (25.05 ± 0.06 µg/mL) after 48 hours of exposure.

1. Introduction

The solvent-free process represents a significant environmental challenge because it offers the potential for producing substances of interest while minimizing the generation of waste.^[1,2] Besides being a sustainable process, it offers the benefits of short reaction times and the ability to operate at room temperature with low-solubility precursors, which would otherwise require large volumes of solvents.^[3] These solvent-free processes are achieved through grinding, milling, shearing, scratching, polishing, or rapid friction.^[4] This study investigates the use of high pressure to conjugate drugs and metal-organic frameworks (MOFs). High pressure promotes the diffusion of drugs into the MOF material eliminating the need for solvents.^[5,6] This solvent-free high pressure may prove superior to that based

on traditional encapsulations,^[7] which rely on large amounts of solvents.

Solvent-free approaches present numerous benefits compared to conventional solvent-based methods, chiefly due to their lower environmental footprint and greater operational efficiency. These techniques decrease the energy usage and streamline experimental workflows.^[8] Furthermore, they often result in faster reaction rates, better selectivity and lower overall costs. By eliminating solvents, these methods significantly cut down on hazardous waste, supporting a cleaner and more sustainable approach to chemical processes.^[9]

The drug, andrographolide (ADG), a diterpene-lactone compound extracted from *Andrographis paniculata*, is widely used to prevent and treat cancer.^[10] However, ADG has a poor water solubility and low bioavailability, although its pharmacological

[a] Dr. W. Pantoja-Romero, Dr. A. Lavín-Flores, Prof. Dr. B. R. Weiner
Department of Chemistry, University of Puerto Rico at Río Piedras Campus,
601 Av. Universidad, San Juan, San Juan, Puerto Rico

[b] Dr. W. Pantoja-Romero, Dr. A. Lavín-Flores, Prof. Dr. G. Morell, Prof.
Dr. B. R. Weiner
Molecular Sciences Research Center, University of Puerto Rico at Río Piedras
Campus, 1390 C. Juan Ponce de León, San Juan 00926, Puerto Rico


[c] Prof. Dr. G. Morell
Department of Physics, University of Puerto Rico at Río Piedras Campus, 601
Av. Universidad, San Juan, San Juan, Puerto Rico


[d] Dr. M. Martínez-Ferrer
Division of Cancer Clinical & Translational Research, University of Puerto
Rico Comprehensive Cancer Center, San Juan 00936, Puerto Rico

[e] Dr. M. Martínez-Ferrer
Department of Pharmaceutical Sciences, School of Pharmacy, University of
Puerto Rico, San Juan 00936-5067, Puerto Rico

[f] Prof. Dr. J. Coronas
Instituto de Nanociencia y Materiales de Aragón (INMA), Universidad de
Zaragoza-CSIC, Zaragoza 50018, Spain
E-mail: coronas@unizar.es

[g] Prof. Dr. J. Coronas
Chemical and Environmental Engineering Department, Universidad de
Zaragoza, Zaragoza 50018, Spain

 Supporting information for this article is available on the WWW under
<https://doi.org/10.1002/chem.202500655>

 © 2025 The Author(s). Chemistry – A European Journal published by
Wiley-VCH GmbH. This is an open access article under the terms of the
[Creative Commons Attribution-NonCommercial-NoDerivs](#) License, which
permits use and distribution in any medium, provided the original work is
properly cited, the use is non-commercial and no modifications or
adaptations are made.

effects are extensive, they are weak, necessitating stringent preparation requirements.^[11] Consequently, developing nanosystems to enhance ADG stability, solubility, and permeability is of critical importance.

MOFs are a class of solid crystalline porous materials composed of metal ions or metallic clusters that serve as nodes and polydentate organic ligands that link these nodes.^[12] The 3D structure of MOFs is formed through strong coordination bonds between the metal ions and organic ligands, creating cavities and inner surfaces occupied by counterions, guest molecules and/or solvate molecules.^[13] Additional interactions, such as hydrogen bonds, metal–metal bonds, and π – π interactions, can also occur and enhance the stability of MOFs.^[14,15] MOFs offer a highly adaptable platform for drug delivery, thanks to their exceptional loading capacity, enhanced stability, bioavailability, controlled release mechanisms, non-toxicity, and responsiveness to specific external stimuli.^[16,17] These features make them well-suited for personalized medicine and improving patient outcomes. In addition, their large pore volumes allow MOFs to either encapsulate therapeutic agents within their frameworks or adsorb them on the surface. For targeted drug delivery, the surface of MOF crystals can be functionalized to serve specific purposes, such as preventing aggregation in the bloodstream or enabling selective recognition of target sites like cancer cells.^[18]

MOFs can be separated into two main families: carboxylate and imidazolate-type MOFs. It is worth highlighting carboxylate-type MOFs like MIL-53(Al), which features a flexible framework, with its internal pore size and volume capable of changing by up to 33% in response to guest molecule adsorption or temperature fluctuations.^[19] Moreover, among the imidazoles, zeolitic imidazolate framework-8 (ZIF-8) is noted for its exceptional thermal and chemical stability, as well as its microporous structure, making it suitable for large-scale industrial applications.^[20]

Drug delivery systems (DDS) are technological platforms designed to formulate and store drug molecules in appropriate forms, like tablets or solutions, for administration. Many of the DDS in use currently involve simple mixing of the drug molecule with edible binders or compatible solvents, depending on the intended route of delivery.^[21] However, these DDS often face several challenges, including inconsistent dosing, low bioavailability, uncontrolled drug release, reduced efficacy, and potential toxicity.^[20,22] To overcome these limitations, advanced DDS should be capable of protecting drugs from harsh environments, enhancing their absorption into the bloodstream and enabling controlled release at specific target sites. In this regard, solvent-free encapsulation methods offer significant advantages, such as improved drug stability against degradation and potential for targeted delivery, avoiding the use of harmful solvents.^[23] Additionally, this approach can enhance drug solubility, increase bioavailability, and support controlled release mechanisms.^[24]

In our laboratory, we previously investigated the incorporation of ADG into MOF pores using a solvent-free method.^[25] However, the MOFs employed were hydrophobic, which did not significantly improve the drug's hydrophilicity. Despite this, their large surface area allowed for the encapsulation of a considerable quantity of the drug.

In this context, carbon-based quantum dots (CBQDs) and their doped counterparts (D-CBQDs) could be utilized to create nanocomposites with ADG. CBQDs are innovative 0D carbon nanomaterials characterized by their small size and relatively strong fluorescence properties. Additionally, CBQDs exhibit good water solubility, chemical stability, resistance to photobleaching, and ease of surface functionalization and they can be prepared on a large scale.^[26,27] In a previous study, some of the current authors conjugated CBQDs and D-CBQDs with ADG, resulting in noticeable changes in the optical and structural properties of these nanomaterials upon interaction with the drug. The findings indicated that conjugating the drug with these nanoparticles significantly improved the affinity of the former for the aqueous phase, reducing the log P (partition coefficient in octanol/water,^[28] which is a parameter used for measuring the lipophilicity of a pharmaceutical compound) from 2.632 to 0.1117.^[29] Consequently, combining MOFs with CBQDs is expected to enhance the hydrophilicity of the composites when combined with ADG.

The presence of ADG in the MOF-CBQD/D-CBQD nanocomposites was studied by scanning electron microscope (SEM), X-ray diffraction (XRD), thermogravimetric analysis (TGA), and Fourier transform infrared (FT-IR) spectroscopy, while their hydrophobicity/hydrophilicity character was monitored with nuclear magnetic resonance (NMR). Finally, to preliminary investigate the cytotoxicity of the materials, a test was performed using human prostate cancer line cells (PC3).

2. Results and Discussion

2.1. Encapsulation of ADG Into Metal-Organic Framework Composites Based on Carbon-Based Quantum Dots and Their Derivatives

XRD is a qualitative method used to monitor the effective loading and/or conjugation of drugs. When guest molecules come into contact with the MOF, their intensity changes due to adsorption within the MOF structure.^[5,6] XRD was employed to investigate the incorporation of ADG into nanocomposites. Figure 1 and Figure S1 show the comparison of the XRD patterns of the MOFs studied herein (MIL-53(Al) and ZIF-8), ADG, CBQD, D-CBQDs, and nanocomposites at room temperature (Table 1).

Structural transitions in flexible MOFs often lead to notable changes in lattice parameters and cell volume, as seen in the benchmark material MIL-53(Al).^[30] However, its crystalline structure remains largely unaffected under high pressure (0.32 GPa), as demonstrated by Monteagudo et al.,^[5] who examined how pressure influences the crystallinity of several MOFs including this one. They calculated the full width at half maximum (FWHM) of the main diffraction peak at 12.5° (corresponding to the (110) plane) before and after pressure exposure. Their results indicated that MIL-53(Al) largely retained its crystallinity despite minor variations in peak intensity, likely due to its inherent flexibility. Additionally, the high-pressure treatment reduced its BET specific surface area from 1140 to 1016 m²/g, suggesting only a limited impact on its microporosity. Conversely, ZIF-8 can

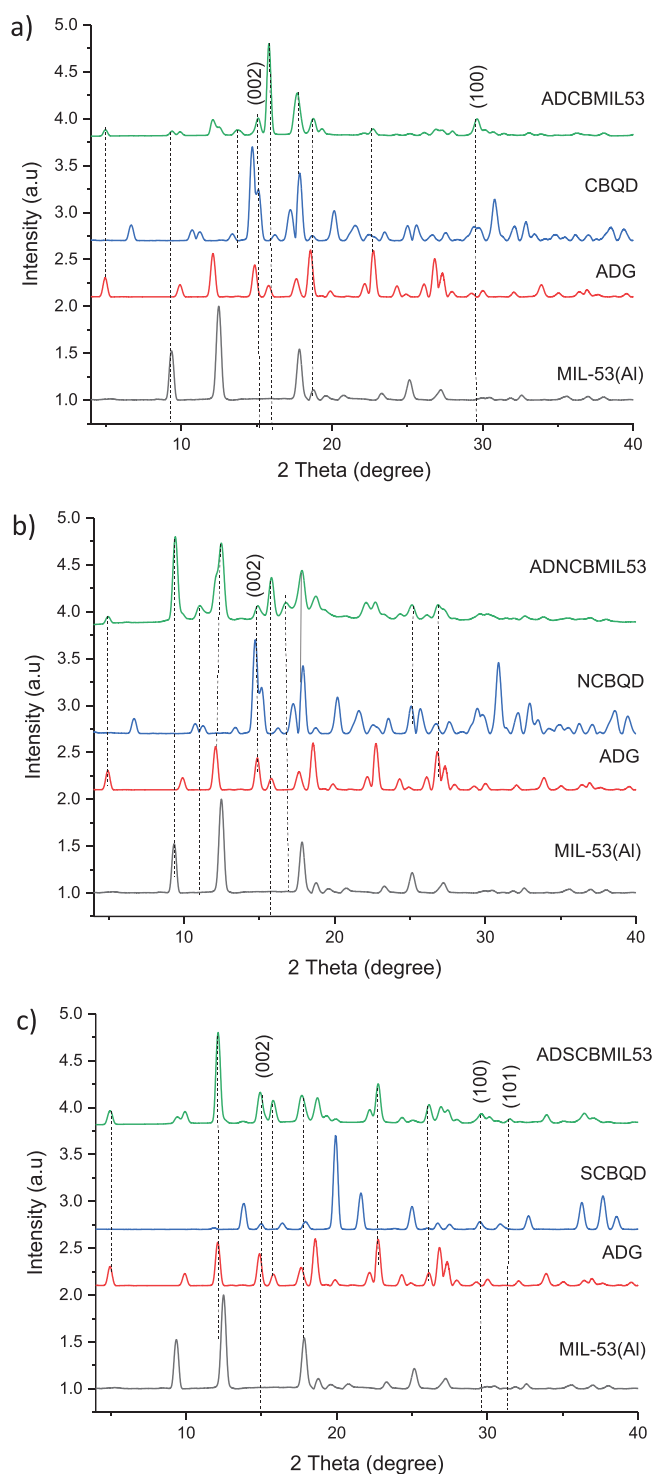


Figure 1. XRD patterns of the different samples (from bottom to top, MOF, ADG, CBQDs, D-CBQD, and nanocomposites after high-pressure encapsulation at room temperature) corresponding to MIL-53(Al): (a) CBQD, (b) NCBQD, and (c) SBQD. Conditions for the encapsulation: room temperature, 0.3 GPa and 1:1:1 MOF/ADG/QD weight ratio.

undergo a phase transition, which is also accompanied by a change in the appearance of the crystal at pressures exceeding 0.8 GPa (much higher than that applied here), forming a previously unidentified phase through a cooperative rearrangement of its framework, reverting upon returning to ambient

Table 1. Nanocomposites based on MOFs and CBQD/D-CBQDs coupling with ADG.

MOF	CBQD/D-CBQD	Nanocomposite
MIL-53(Al)	CBQD	ADCBMIL
MIL-53(Al)	N-CBQD ^[a]	ADNCBMIL
MIL-53(Al)	S-CBQD ^[b]	ADSCBMIL
ZIF-8	CBQD	ADCBZIF8
ZIF-8	N-CBQD ^[a]	ADNCBZIF8
ZIF-8	S-CBQD ^[b]	ADSCBZIF8

^[a] Carbon-based quantum dots doped with nitrogen.

^[b] Carbon-based quantum dots doped with sulfur.

pressure.^[31] Based on these observations, these two types of MOFs were selected to encapsulate the drug ADG.

Figure 1a shows that ADCBMIL presents XRD intensities corresponding to the characteristic graphite planes (002) and (100) at 15° and 29°, respectively, along with a noticeable increase in the ADG peak at 15° related to the plane (012). Also, Figure 1b shows that ADNCBMIL exhibits one characteristic graphite plane (002) at 15° and a noticeable increase in the ADG peak at 12° (100). However, ADSCBMIL, despite showing a noticeable increase in the ADG peak at 12° (100), like ADNCBMIL, displays all characteristic graphite planes (002), (100) and (101) (Figure 1c). As stated before, encapsulation in MOFs leads to a decrease in the signals of the encapsulated drug,^[5,6,32] so that if this is encapsulated in the porous volume of the host (i.e., the MOF), not impregnating its external surface (as when conjugating with the QDs), the guest XRD signals should not appear in the corresponding pattern. It is important to note that ADG is not only adsorbed on the MOF porosity but also conjugated with CBQDs and D-CBQDs. This implies that some amount of the drug is encapsulated within the pores of the MOFs, evidenced by the decrease in the main ADG peak at 10° (002) when comparing the XRD patterns of all nanocomposites. Additionally, some amount of the drug appears to be impregnated outside of the pores of the MOFs, likely conjugating with CBQDs and D-CBQDs, as demonstrated in a previous study.^[29] Moreover, new planes in the XRD patterns of all nanocomposites can be attributed to polar functional groups of ADG interacting with the external functional groups of QDs through electrostatic, H-bonding, and/or $\pi-\pi$ stacking interactions.^[33]

In ADCBZIF8, signs of CBQD or ADG are barely noticeable. This suggests that neither the drug nor the CBQD is fully conjugated, with only the MOF undergoing any transformation (Figure S1a). However, ADNCBZIF8 displays characteristic graphite planes (002), (100) and (101) (Figure S1b), while ADSCBZIF8 shows two characteristic graphite planes (002) and (100) (Figure S1c). ADNCBZIF8 and ADSCBZIF8 exhibit a significant reduction in the ADG peak at 12° (100). The reduction of the intensities corresponding to ZIF-8 in its nanocomposites can be attributed to the drug adsorption in the MOF pores and some interaction with the D-CBQDs. It is worth noting that the pressure itself appears to affect the crystal pattern of ADG, enhancing the ADG peak intensity at around 12.0° as compared to the other intensities. This

may be due to crystal modifications resulting from high-pressure exposure, a phenomenon seen in some drugs that can lead to new crystal habits, metastable polymorphic forms, or a reduction in the degree of crystallinity.^[34,35] Despite these changes, the encapsulated drug retains its characteristic peaks, with the 2-theta values remaining unaffected by pressure.

Thermal stabilization of ADG after conjugation, related to its adsorption on the MOF porosity and coupling with CBQD and D-CBQDs, was observed through TGA (Figures S2 and S3). MIL-53(Al) shows a low-temperature loss of adsorbed water within the pores, while the higher temperature step corresponds to the decomposition of the terephthalate ligand from the MOF framework. ADG exhibited an initial 2.1% weight loss between 120 °C and 147 °C due to the evaporation of bound water.

The major weight loss of 80.4% occurred between 253 °C and 438 °C, attributed to the decomposition of ADG (since its boiling point is at ca. 557 °C) and disruption and degradation of chemical bonds in the remains at above 438 °C, leaving an undetectable residue.^[36,37] Figure S2a shows that in the first stage (0–150 °C), CBQD experienced a 16.4% weight decrease, likely due to the evaporation of adsorbed water and small molecules connected via weak hydrogen bonds in the samples. In the second stage (150–250 °C), a 13.0% weight loss likely corresponds to the degradation of carboxyl groups (–COOH). The final decomposition step occurred at 350–700 °C, likely due to the depletion of residual carbons under high temperatures.^[38] ADCBMIL displays, in the first stage (around 200 °C), the loss of the solvent contained in the samples. The second stage (300–400 °C) can be attributed to the initial losses of ADG and CBQD. The third stage (400–500 °C) is due to the loss of oxygen and hydroxyl groups from ADG and CBQD. Finally, above 500 °C, residues of CBQD and MIL-53(Al) are present, likely in the form of Al₂O₃. Figure S2b shows that in the first stage (0–150 °C), NCBQD involved the removal of hydroxyl, carboxyl and amide groups.^[39] In the second stage (150–250 °C), there was a 14.0% weight loss. During the third stage (250–350 °C), a 16.0% weight loss occurred, possibly due to the gradual decomposition of other organic functional groups (–OH) and the elimination of phenyl groups.^[40]

The final decomposition step, which occurred at 350–700 °C, likely resulted from the depletion of residual carbons under high temperatures and the elimination of pyridine and pyrrolidine groups in NCBQD, resulting in a total weight loss of ca. 8.0%. ADNCBMIL, in the first stage (0–150 °C), shows the loss of the solvent contained in the samples. The second stage (150–250 °C) can be attributed to initial losses of ADG. The third stage (250–400 °C) involves the loss of ADG and NCBQD. The fourth stage (400–550 °C) is due to the loss of oxygen and hydroxyl groups from ADG, NCBQD, and MIL-53(Al). Figure S2c shows that in SCBQD, a weight loss of 6.3% was observed at 0–100 °C, likely due to the evaporation of adsorbed water. At 120–400 °C, a significant weight loss of 90.0% occurred, indicating the elimination of sulfur, thus confirming the sulfur content in SCBQD.^[41] ADSCMIL displays, in the first stage (0–100 °C), the loss of the solvent contained in the samples. The second stage (100–250 °C) can be attributed to initial losses of SCBQD, indicating the evaporation of sulfur. The third stage (250–550 °C) can be attributed to losses corresponding to the remaining amount of ADG. The last stage

(above 550 °C) is due to the loss of oxygen and hydroxyls in SCBQD and MIL-53(Al) and final decomposition of the remains.

ZIF-8 has a small weight loss in the temperature range of 100–400 °C, indicating that ZIF-8 was stable up to 400 °C. The major weight loss of ZIF-8 takes place in the range of 450–600 °C and can be ascribed to the decomposition of the 2-methylimidazolate ligand (Figure S3a,b, and c). In the TGA curves for ADCBZIF, the first stage of weight loss is due to the evaporation of adsorbed water and small molecules connected via weak hydrogen bonds in the samples. ZIF-8 is hydrophobic, thus, the water interaction is due to the presence of the QDs in the nanocomposites. The second stage (180–400 °C) is due to the losses of ADG and CBQD, as well as the loss of oxygen and hydroxyl groups. In the last stage (450–550 °C), residues of CBQD and ZIF-8 are present (Figure S3a). ADNCBZIF, in the first stage (0–150 °C), shows the loss of the solvent contained in the samples. The second stage (150–400 °C) can be attributed to initial losses of ADG and NCBQD. The third stage (400–550 °C) is due to the loss of oxygen and hydroxyl groups from ADG and NCBQD and final decomposition of the remains (Figure S3b). ADSCZIF displays, in the first stage (0–100 °C), the loss of the solvent contained in the samples. The second stage (100–250 °C) can be attributed to initial losses of SCBQD, indicating the evaporation of sulfur. The third stage (250–550 °C) can be attributed to initial losses of ADG. The last stage (above 550 °C) can be described as well as done above (Figure S3c).

SEM has been used to analyze the shape and structure of nanocomposites. The morphology studies of ADCBMIL, ADNCBMIL, and ADSCBMIL revealed that they were homogeneous and irregular in shape (Figure 2a,c, and e). EDS analysis confirmed the presence of carbon, oxygen, and aluminum (from MOF) in all nanocomposites, while the presence of sulfur was specifically detected in ADSCBMIL (Figure 2b,d, and f). Notably, the doped nanocomposites exhibited a more dispersed shape, likely due to the larger size of nitrogen and sulfur atoms compared to carbon.^[29] ADCBZIF and ADSCBZIF (Figure S4a and c) displayed a more homogeneous and regular shape compared to ADSCBZIF (Figure S4e). EDS analysis confirmed the presence of carbon, oxygen, and zinc (from MOF) in all nanocomposites, while nitrogen and sulfur atoms were specifically identified in ADNCBZIF and ADSCBZIF, respectively (Figure S4b,d, and f).

Both MOFs and CBQDs/D-CBQD exhibit high crystallinity, as demonstrated by XRD characterization, making them suitable for the encapsulation/conjugation of ADG at high pressure. Changes in crystal sizes can be attributed to pressure and different compositions of the nanocomposites.

FTIR measurements were conducted to identify the structural changes in the materials obtained from the conjugation of ADG, MOFs, and CBQDs/D-CBQD. Figure 3 compares ADG, MIL-53(Al), and ADG-CBQD/D-CBQD subject to high pressure at room temperature. ADCBMIL displays peaks at 3500, 3300, 1608, and 1512 cm^{−1}, corresponding to the C–H, O–H, asymmetric COO group, symmetric stretching of the –COO group, O–H for primary and secondary alcoholic functions, associated with CBQD. Peaks at 1220 cm^{−1} are attributed to the presence of the C–O–C of the lactone ring of ADG (Figure 3a). ADNCBMIL shows peaks at 1458 and 1220 cm^{−1}, also due to the C–O–C in the lactone

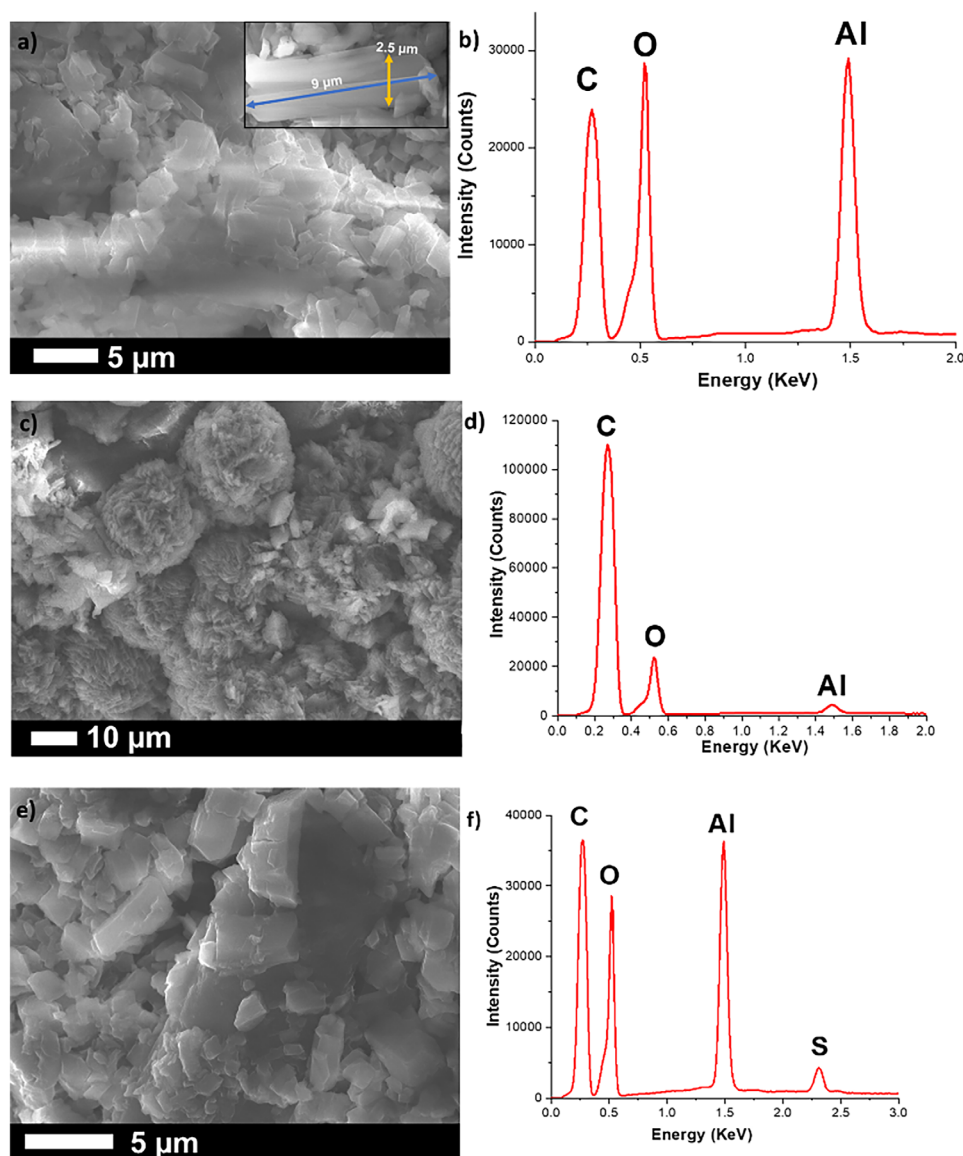


Figure 2. SEM images and EDS analyses of (a,b) ADCBMIL, (c,d) ADNCBMIL, and (e,f) ADSCBMIL. Conditions for the encapsulation: room temperature, 0.3 GPa and 1:1:1 MOF/ADG/QD weight ratio.

ring of ADG (Figure 3b). ADSCBMIL exhibits few signals indicative of both SCBQD and ADG. However, it is notable that peaks at 1043 and 875 cm^{-1} correspond to the C—O—C groups in the lactone ring, which is present in the molecular structure of ADG (Figure 3c). These samples exhibit shifts in the C=O band of the conjugated samples compared to bare ADG (1727 cm^{-1}), confirming that the chemical bonds in the ADG molecules remain unchanged, whether encapsulated in the MOF microporosity or coupled with CBQD/DCBQD. This observation is consistent with the formation of a hydrogen bond between the carboxylic group of MIL-53(Al) and the hydroxyl group of ADG.

NMR is a well-established technique for investigating various types of porous materials. NMR has been successfully employed to characterize the structure of these materials and study host-guest interactions in MOFs.^[42–44] In this study, ^1H NMR was utilized to explore the interactions between ADG, CBQD/D-CBQDs, and MOFs.

The observed signals in the ^1H NMR, when comparing CBQDs/D-CBQDs, MIL-53(Al), and ADG with those of the nanocomposites, confirmed the conjugation of these materials. For ADCBMIL, signals were observed at 7.81 and 6.53 ppm, corresponding to the aromatic protons of MIL-53(Al) and CBQD, respectively. Signals at 3.28–3.04 ppm were attributed to protons present in ADG. Additionally, shifts were noted around 2.44–2.62 ppm when compared with CBQD (Figure 4). Similarly, ADNCBMIL (Figure S5) showed signals at 7.81 and 6.53 ppm corresponding to the aromatic protons of MIL-53(Al) and NCBQD, respectively. Shifts around 2.44–2.62 ppm were again observed when compared with NCBQD (Figure S6). For ADSCBMIL (Figure S7), a signal at 7.81 ppm was observed, corresponding to the aromatics protons of MIL-53(Al), while the signal at 6.53 ppm corresponds to the vinylic protons of ADG. Shifts were noted around 2.44–2.62 ppm when compared with SCBQD (Figure S8).

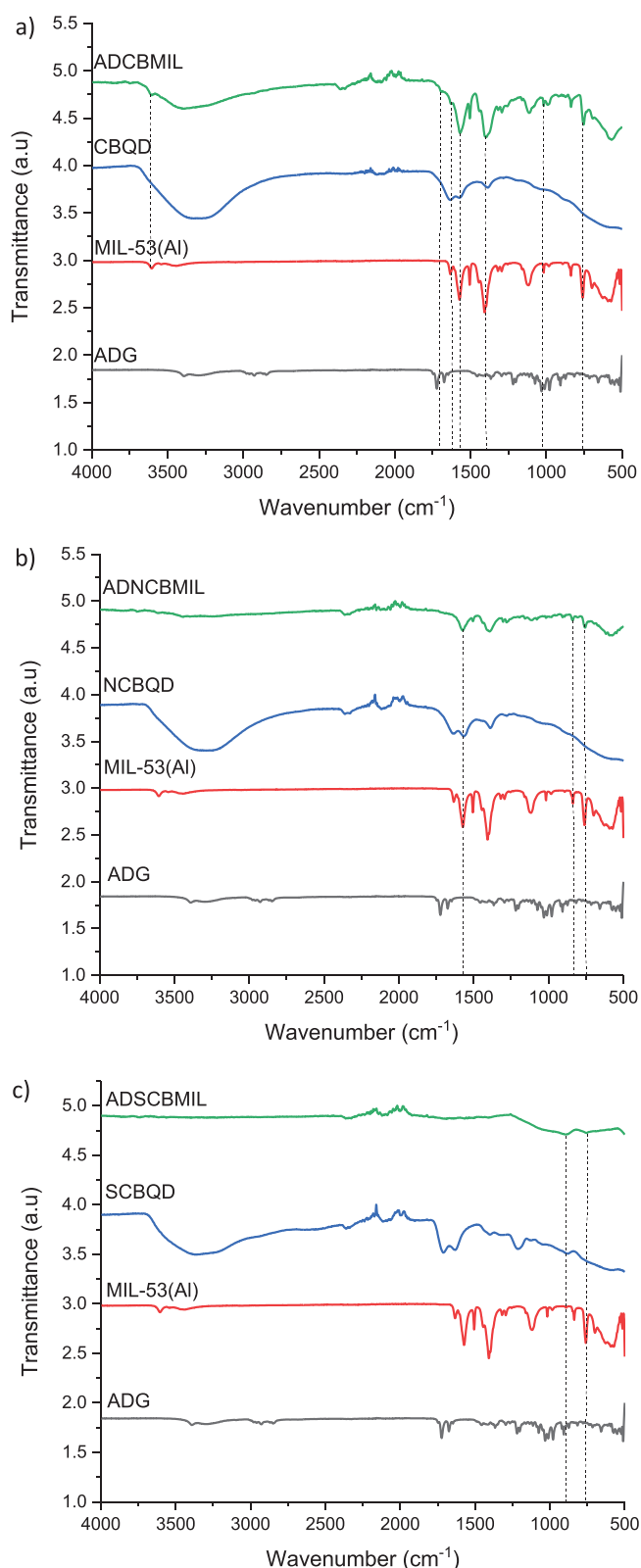


Figure 3. FT-IR of the different samples from bottom to top, ADG, MIL-53(Al), and ADG-CBQD/D-CBQD: (a) CBQD, (b) NBQDs, and (c) SBQDs. Conditions for the encapsulation: room temperature, 0.3 GPa, and 1:1:1 MOF/QD/ADG weight ratio.

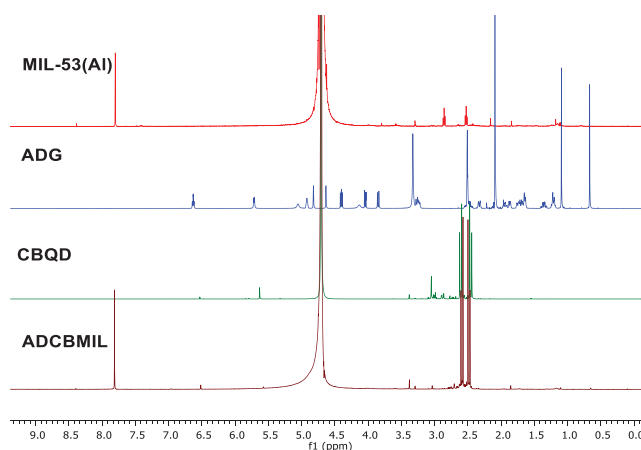


Figure 4. ^1H NMR spectra comparison of the different samples from bottom to top, ADCBMIL, CBQD, ADG, and MIL-53(Al). Conditions for the encapsulation: room temperature, 0.3 GPa, and 1:1:1 MOF/QD/ADG weight ratio.

Conversely, ADCBZIF exhibits signals at 6.96 and 6.50 ppm, corresponding to the allylic protons of ZIF-8 and CBQD, respectively. Additionally, methylene protons of ZIF-8 at 2.42 ppm were observed. Signals at 1.10, 3.37, and 4.0 ppm were observed corresponding to ADG (Figure S9). Similarly, ADNCBZIF and ADSCBZIF exhibit signals at 6.96 and 6.50 ppm, corresponding to the allylic protons of ZIF-8, NCBQD/SCBQD, respectively. Shifts around 2.44–2.62 ppm were noted when compared with NCBQD and SCBQD (Figures S10 and S11).

2.2. Partition Coefficient and General Solubility Equation (GSE) Studies

The hydrophobic and hydrophilic properties, expressed in terms of $\log P$, were examined for all nanocomposites conjugated with ADG. Given that ADG is insoluble in water, the synthesized nanocomposites are expected to enhance its solubility for effective delivery to cancerous cells. The $\log P$ values indicate the compound nature: hydrophilicity (ranging from 0 to -2), hydrophobicity (ranging from 0 to 2) and amphiphilic (0).^[45]

$\log P$ results obtained using ^1H NMR with D_2O at a neutral pH as the aqueous phase showed that by conjugating ADG with CBQDs/D-CBQDs and MOFs, the hydrophilicity improved notably (Figure 5) compared to being encapsulated only in the pores of the MOFs previously (i.e., with not QDs, see Table S1).

ADCBMIL showed the greatest improvement in solubilizing ADG, followed by ADSCBMIL, and finally ADNCBMIL. The variations in performance between the doped and undoped nanocomposites are attributed to differences in surface defects, as previously demonstrated in the coupling of ADG with CBQDs/DCBQDs.^[29] It is important to note that the hydrophobicity of MOFs is characterized by their contact angles with water (WCA).^[46,47] MIL-53(Al), for instance, is slightly hydrophilic due to a free $-\text{OH}$ group linked to aluminum and has a contact angle of 86° ,^[48] which results in lower hydrophilicity of the ADG when conjugated with this MOF compared to ZIF-8, which

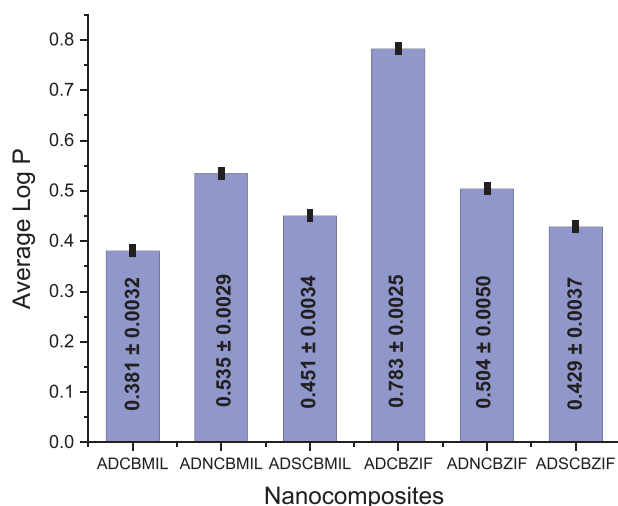


Figure 5. Histograms for log P tests by ^1H NMR method for MOFs/CBQD-DCBQDs/ADG nanocomposites.

Table 2. Results for GSE calculations of ADG/CBQD/D-CBQDs/MOFs nanocomposites.

Material	Log P	S_w [$\mu\text{g/mL}$]	Ratio [S_w MOFs-ADG-CBQDs/ S_w ADG]
ADG	1.106	22.5 ^[39]	N/A
ADCBMIL	0.381	4006	178
ADNCBMIL	0.535	2812	125
ADSCBMIL	0.451	3414	152
ADCBZIF	0.783	1590	71
ADNCBZIF	0.504	3023	134
ADSCBZIF	0.429	3593	160

has a contact angle of 142° .^[49] Consequently, ADCBZIF showed less improvement in solubilizing ADG than ADCBMIL. Similarly, ADSCBZIF and ADNCBZIF follow the same solubility trend as ADSCBMIL and ADNCBMIL (Figure 5). Despite this, the log P value of ADG, originally 1.106 ± 0.018 , improved in all nanocomposites when conjugated. Furthermore, the hypothesis of enhancing solubility by adding CBQDs/D-CBQDs to the MOFs previously studied with ADG was successfully validated.

GSE is a dependable approach for estimating the molar aqueous solubility (S_w) of nonelectrolytes,^[50] providing insight into potential solubility trends. Table 2 presents GSE results for estimating the water solubility of MOFs/CBQD-DCBQDs/ADG nanocomposites. It can be noted that there was a significant increase in the solubility of ADG conjugated in the nanocomposites compared to the ADG S_w using its log P from literature for the GSE.^[51] To calculate the LogP and GSE, Equations (S1)–(S3) found in the supporting information were used. The ratio (last column of Table 2) is the relative size of two quantities expressed as the quotient of one divided by the other, that is, the solubility of a given composite material (S_w) compared to that of the drug ($S_w = 22.5 \mu\text{g/mL}$). These findings align with those observed in log P measurements and can be explained by the

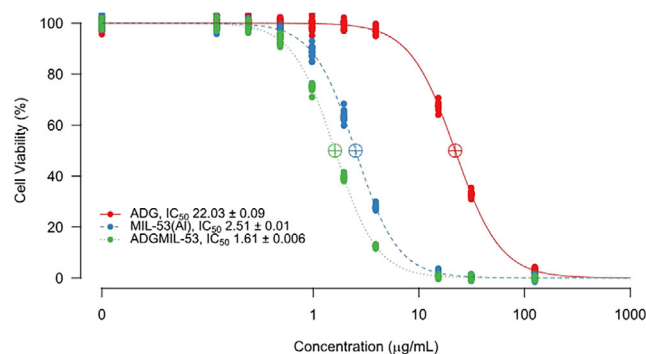


Figure 6. IC_{50} curves for MIL-53(Al) (blue line), ADG (red line) and ADGMIL-53 (green line) using PC3 cell line at 48 h of treatment.

combination of ADG/MOFs with CBQDs/DCBQDs. The excellent solubility of CBQDs/DCBQDs facilitates the formation of soluble nanocomposites through $\pi-\pi$ interactions. The inherent presence of polar residues on the CBQDs/DCBQDs surface provides them with good solubility in water, which is particularly useful for applications in nanobiology or nanomedicine,^[52] especially for hydrophobic drugs like ADG.

3. Cytotoxicity Assays

Preliminary cytotoxicity tests of the MOFs, the loaded MOFs and AGD were performed at 48 h of treatment using cell line PC3 corresponding to human prostate cancer (Figures 6 and S12). The cell line PC3, androgen-independent grade IV adenocarcinoma, produces prostate-specific antigen (PSA) but does not express an androgen receptor (AR).^[53,54] Notably, ZIF-8 (Figure S12) had a lower IC_{50} compared to MIL-53(Al) (Figure 6), which can be attributed to its composition of zinc clusters connected to the imidazolate linkers through coordination bonding, potentially leading to accumulation in the body depending on the metal concentration.^[55] Cancer cells naturally have higher levels of reactive oxygen species (ROS) than normal cells due to their role in tumor development.^[56] ROS are chemically reactive molecules that contain oxygen and are produced in living organisms. The influence of ZIF-8 concentrations on cell viability may be attributed to the release of Zn^{2+} into the cell media, which induces ROS generation and activation of apoptosis pathways.^[57–59] The ROS generation plays an important role in the proliferation and survival of cells, as has been reported.^[60–62] However, since the current study did not evaluate the release of Zn ions into the cell media, the findings should be judged with caution and further study needs to be done to examine the toxicity mechanisms of ZIF-8.

Conversely, as hypothesized, the encapsulated MOFs demonstrated significantly better performance in cytotoxicity compared to MOFs alone or ADG ($22.03 \pm 0.09 \mu\text{g/mL}$) itself. The IC_{50} values for each compound were $1.61 \pm 0.006 \mu\text{g/mL}$ for ADGMIL-53 (Figure 6) and $4.01 \pm 0.02 \mu\text{g/mL}$ for ADGZIF-8 (Figure S12). ADG encapsulated in the ADGMIL-53 exhibited a much steeper response compared to its encapsulation in ZIF-8, indicating greater drug sensitivity and response. The release profile of

drugs encapsulated in nanocarriers is a critical aspect to consider. The data suggest that the release dynamics of the drug from ZIF-8 might have contributed to the slow reduction in cytotoxicity compared to ZIF-8 alone. In contrast, MIL-53(Al) showed a high percentage of initial ADG released (about 80%) at 37 °C after 30 h, suggesting a strong ADG — MIL-53(Al) affinity as previously reported in our laboratory.^[25]

4. Conclusion

ADG/MOFs/CBQDS-DCBQDs were successfully synthesized using a solvent-free method under high pressure. Characterization through XRD patterns, TGA curves, UV-vis, FT-IR, SEM, and solid-state ¹H NMR spectra confirmed the effective conjugation of all components. The results indicated that ADG was partially encapsulated within the MOF pores, while another portion was bound externally to CBQD/DCBQDs, as evidenced by distinct drug signals in each analysis. MOFs and loaded MOFs exhibited cytotoxic effects against cancer cells. Among them, ZIF-8 showed a lower IC₅₀ compared to MIL-53(Al), likely due to its structure of zinc clusters coordinated with imidazoles, which facilitate the release of Zn²⁺ ions into the cell medium promoting the generation of ROS. It is crucial to conduct cytotoxicity studies on the nanocomposites comprising MOFs, CBQDs, and D-CBQDs combined with ADG in PC3 type cells, followed by evaluations in normal human prostate cells.

Finally, this green synthesis approach simplified the conjugation process and significantly enhanced the drug solubility, as indicated by changes in hydrophobicity observed via ¹H NMR, surpassing ADG encapsulation within MOFs. The conjugated nanosystem opens up new avenues for more effective therapeutic applications of ADG.

5. Experimental Section

Synthesis of MIL-53(Al): Following a previous report for the synthesis of MIL-53(Al),^[63] 5.2 g (13.9 mmol) of aluminum nitrate nonahydrate (Sigma Aldrich, 98%) and 1.12 g (6.7 mmol) of terephthalic acid (Sigma Aldrich, 98%) were dissolved in 20 mL of distilled water and placed in a Teflon-lined steel autoclave for 3 days at 220 °C. The product was recovered by centrifugation at 10,000 rpm for 10 min, washed once with ethanol by centrifugation under the same conditions and dried overnight at 65 °C. The solid was activated by calcination at 380 °C for 24 h.

Synthesis of ZIF-8: To obtain ZIF-8,^[64] two different solutions were prepared. First, 2.93 g (9.87 mmol) of zinc nitrate hexahydrate (Sigma Aldrich, 98%) was dissolved in 200 mL of methanol in a spherical flask. Secondly, 6.489 g of 2-methylimidazole (79.04 mmol) in 200 mL of MeOH was prepared in parallel. The former solution was then added to the latter and stirred at room temperature for 30 min. The product was centrifuged at 8,000 rpm for 15 min and washed twice with 50 mL of fresh MeOH. The final product was then dried overnight at either room temperature or 70 °C.

Conjugation of ADG with MIL-53(Al), ZIF-8, CBQD, and D-CBQD: The conjugation was carried out using a high-pressure technique.^[65]

Equal weights (75 mg each) of CBQD or D-CBQD (NCBQD and SCBQD), MOFs (ZIF-8 or MIL-53(Al)), and ADG (1:1:1 weight ratio) were combined and thoroughly mixed by hand-shaking in a vial for 1 min. The resulting mixture was transferred to a metal cylinder of a hydraulic press (YLJ 15T, MTI Corporation) and maintained at room temperature. The press was used to compact the mixture under a pressure of 0.3 GPa for 15 min using a metal piston.

Cytotoxicity studies in PC3 cancer cells: Human androgen-independent prostate cancer cells PC3 were purchased from American Type Culture Collection (ATCC), (Manassas, VA, USA), CRL-1435. This product is intended for laboratory research use only.

Cell culture: PC3 cells were incubated at 37 °C in a humidified atmosphere with 5% CO₂ using media containing either 0.05% Trypsin–0.53 mM EDTA solution diluted 1:1 with D-PBS, 0.1% Soybean Trypsin Inhibitor, or 2% fetal bovine serum (FBS) in D-PBS. Cell passaging was conducted weekly when cultures reached 80%–90% confluency. The media was refreshed twice per week.

Cell seeding: PC3 cells were seeded into 96-well plates at a density of 7.0×10^4 cells/mL. The plates were incubated at 37 °C in a humidified environment containing 5% CO₂ for 24 h. Three replicate 96-well plates were prepared for each time point (48 h).

Cell treatments: To determine the IC₅₀ values, two-fold serial dilutions of MIL-53(Al), ZIF-8 (0–125 µg/mL), ADGMIL-53, ADGZIF-8 (0–125 µg/mL), and ADG (0–500 µg/mL) were prepared. Treatments were applied after 24 h of initial cell incubation. All treatments were administered 24 h after cell seeding. For each well, 100 µL of the prepared solution was added and cells were incubated with the treatments for 48 h to determine the IC₅₀ values. The control group received only culture media (RPMI or F-12 supplemented with 1% Pen-Strep). All experiments were conducted in triplicate.

MTS assay: Cell proliferation was assessed after 48 h of treatment using the MTS assay. An MTS solution in RPMI was prepared according to the number of 96-well plates to be processed. After treatment, the media was removed from all wells and 100 µL of the MTS solution was added to each well. Plates were incubated for 4 h at 37 °C. Fluorescence was measured at an excitation wavelength of 560 nm and an emission maximum (λ_{max}) of 590 nm. Cell viability was expressed as a percentage relative to the control group (set at 100%) and compared across cells treated with material solutions.

Statistical analyses were performed using the R open-source environment. Dose–response relationships were evaluated with the typical dose–response curve package, treating blank samples as having a dose of 0 µg/mL. IC₅₀ values were calculated from the fitted curve parameters.

Supporting Information

Supporting information about experimental details (including the legal disclaimers done by the seller of the cancer cells) and additional XRD, TGA, SEM, NMR and IC₅₀ results. The authors have cited additional references within the Supporting Information.^[28,50,66]

Acknowledgements

This research was carried out under the auspices of the Fundación Carolina España, PR NASA EPSCoR (NASA Cooperative Agreement [NNX15AK43A]). We also acknowledge funding in part from the National Institutes of Health/National Cancer Institute under Grant #U54 CA096297. This work acknowledges grants PID2022-138582OB-I00 (funded by MCIN/AEI/10.13039/501100011033/ and by “ERDF A way of making Europe”) and CEX2023-001286-S (funded by MICIU/AEI/10.13039/501100011033) and grant T68-23R from the Aragón Government.

Conflict of Interests

The authors declare no conflict of interest.

Data Availability Statement

The data that support the findings of this study are available in the supporting information of this article.

Keywords: high-pressure chemistry · metal-organic frameworks · organic-inorganic hybrid composites · quantum dots

- [1] A. Pichon, A. Lazuen-Garay, S. L. James, *CrystEngComm* **2006**, *8*, 211.
- [2] G. Kaupp, J. Schmeyers, J. Boy, *Chemosphere* **2001**, *43*, 55.
- [3] T. Friscic, *J. Mater. Chem.* **2010**, *20*, 7599.
- [4] G. Kaupp, *CrystEngComm* **2009**, *11*, 388.
- [5] R. Monteagudo-Olivan, L. Paseta, G. Potier, P. López-Ram-de-Viu, J. Coronas, *Eur. J. Inorg. Chem.* **2019**, *2019*, 29.
- [6] B. Zornoza, C. Rubio, E. Piera, M. A. Caballero, D. Julve, J. Pérez, C. Téllez, J. Coronas, *ACS Appl. Mater. Interfaces* **2022**, *14*, 22476.
- [7] P. Horcajada, C. Serre, V.-R.-M., M. Sebban, F. Taulelle, G. Férey, *Angew. Chem., Int. Ed.* **2006**, *45*, 5974.
- [8] M. Jee, S., C. Ahn, H. Park, J., A. Kim, T., M. Park, *Compos. B Eng.* **2020**, *202*, 108438.
- [9] J. Ye, X. Tang, L. Cheng, S. Zhang, W. Zhan, Y. Guo, L. Wang, X.-M. Cao, X.-M. Wang, X.-M. Wang, S. Dai, Y. Guo, *ACS Appl. Mater. Interfaces* **2024**, *16*, 1944.
- [10] B. Zeng, A. Wei, Q. Zhou, M. Yuan, K. Lei, Y. Liu, J. Song, L. Guo, Q. Ye, *Phytother Res.* **2022**, *36*, 336.
- [11] W. Sun, L. D. Du, S. B. Wang, X. P. Chen, G. H. Du, in: *Natural Small Molecule Drugs from Plants*, Springer, Singapore **2018**, pp. 731–736.
- [12] D. Britt, D. Tranchemontagne, O. M. Yaghi, *Proc. Natl. Acad. Sci.* **2008**, *105*, 11623.
- [13] Y. Wang, X.-G. Wang, B. Yuan, C.-Y. Shao, Y. Y. Chen, B.-b. Zhou, M.-S. Li, X.-M. An, P. Cheng, X.-J. Zhao, *Inorg. Chem.* **2015**, *54*, 4456.
- [14] G. Férey, M. Haouas, T. Loiseau, F. Taulelle, *Chem. Mater.* **2014**, *26*, 299.
- [15] C. P. Raptoupoulou, *Materials (Basel)* **2021**, *14*, 310.
- [16] D. S. R. Khafaga, M. T. El-Morsy, H. Faried, A. H. Diab, S. Shehab, A. M. Saleh, G. S. M. Ali, *RSC Adv.* **2024**, *14*, 30201.
- [17] S. He, L. Wu, X. Li, H. Sun, T. Xiong, J. Liu, C. Huang, H. Xu, H. Sun, W. Chen, R. Gref, J. Zhang, *Acta Pharm. Sin. B* **2021**, *11*, 2362.
- [18] P. Patil, G. Basarkar, S. Patil, *Int. J. of Pharm. Sci.* **2025**, *3*, 1100.
- [19] J. Warfsmann, B. Tokay, N. R. Champness, *CrystEngComm* **2018**, *20*, 4666.
- [20] M. Bergaoui, M. Khalfaoui, M. Awadallah-F, S. Al-Muhtaseb, *J. Nat. Gas Sci. Eng.* **2021**, *96*, 104289.
- [21] T. C. Ezike, U. S. Okpala, U. L. Onoja, C. P. Nwike, E. C. Ezeako, O. J. Okpara, C. C. Okoroafor, S. C. Eze, O. L. Kalu, E. C. Odoh, U. G. Nwadike, J. O. Ogbodo, B. U. Umeh, E. C. Ossai, B. C. Nwanguma, *Heliyon* **2023**, *9*, e17488.
- [22] S. Adepu, S. Ramakrishna, *Molecules* **2021**, *26*, 5905.
- [23] M. Sun, M. Gao, J. Bi, Y. Zhao, J. Gong, *ACS Sustainable Chem. Eng.* **2024**, *12*, 4813.
- [24] L. Becker-Peres, L. Becker-Peres, P. H. Hermes de Araújo, C. Sayer, *Colloids Surf., B* **2016**, *140*, 317.
- [25] W. Pantoja-Romero, Y. Aysa-Martínez, A. Lavín-Flores, N. Medina-Berrios, M. Bayro, G. Morell, B. R. Weiner, J. Coronas, *Eur. J. Inorg. Chem.* **2024**, *27*, e202400511.
- [26] S. Zhu, Y. Song, X. Zhao, J. Shao, J. Zhang, B. Yang, *Nano Res.* **2015**, *8*, 355.
- [27] S. Yang, J. Sun, X. Li, W. Zhou, Z. Wang, P. He, *J. Mater. Chem. A* **2014**, *2*, 8660.
- [28] H. Cumming, C. Rücker, *ACS Omega* **2017**, *2*, 6244.
- [29] N. Medina-Berrios, & W. Pantoja-Romero, L. Flores, A., D. Vélez, C. S. M. Guadalupe, C. A. T. Mulero, T. M. K. Kisslinger, M. Martínez-Ferrer, G. Morell, B. R. Weiner, *ACS Omega* **2023**, *9*, 12575.
- [30] A. Schneemann, V. Bon, I. Schwedler, I. Senkovska, S. Kaskel, R. A. Fischer, *Chem. Soc. Rev.* **2014**, *43*, 6062.
- [31] S. A. Moggach, T. D. Bennet, A. K. Cheethan, *Angew. Chem., Int. Ed.* **2009**, *48*, 7087.
- [32] Liédana, N., Galve, A., Rubio, C., Téllez, C., Coronas, J., *ACS Appl. Mater. Interfaces* **2012**, *4*, 5016.
- [33] S. Das, A. Halder, S. Mandala, M. Mazumder, T. Bera, A. Mukherjee, P. Roy, *Artif Cells Nanomed Biotechnol* **2018**, *46*, S751.
- [34] B. Ibraheem, K. G. Wagner, *Int. J. Pharm. X.* **2021**, *3*, 100075.
- [35] D. Braga, L. Casali, F. Grepioni, *Int. J. Mol. Sci.* **2022**, *23*, 9013.
- [36] G. Zhao, Q. Zeng, S. Zhang, Y. Zhong, C. Wang, Y. Chen, L. Ou, Z. Liao, *Pharmaceutics* **2019**, *11*, 74.
- [37] S. Y. Lee, L. C. Abdullah, R. Abdul Rahman, F. Abas, W. K. Tan, C. Gun Hean, *Chem. Eng. Res. Des.* **2018**, *138*, 176.
- [38] V. N. Mehta, S. Jha, R. K. Singhal, Kailasa, S. K., *New J. Chem.* **2014**, *38*, 6152.
- [39] B. Senel, N. Demir, G. Büyükköroğlu, M. Yıldız, *Saudi Pharma. J.* **2019**, *27*, 846.
- [40] J. Tang, J. Zhang, W. Zhang, Y. Xiao, Y. Shi, F. Kong, W. Xu, *J. Mater. Sci. Technol.* **2021**, *83*, 58.
- [41] R. Du, Z. Shi, C. Yu, W. Rao, C. Xu, J. Wang, *Ionics* **2021**, *27*, 4269.
- [42] H. Koller, M. Weiss, *Top. Curr. Chem.* **2012**, *306*, 189.
- [43] W. Zhang, S. Xu, X. Han, X. Bao, *Chem. Soc. Rev.* **2012**, *41*, 192.
- [44] M. Eddaoudi, J. Kim, N. Rosi, D. Vodak, J. Wachter, M. O’Keefe, O. Yaghi, *Science* **2002**, *295*, 469.
- [45] I. Moriguchi, S. Hirono, I. Nakagome, H. Hirano, *Chem. Pharm* **1994**, *42*, 976.
- [46] L. H. Xie, M. M. Xu, X. M. Liu, M. J. Zhao, J. R. Li, *Adv. Sci.* **2020**, *7*, 1901758.
- [47] S. Mukherjee, S. Sharma, S. K. Ghosh, *APL Mater.* **2019**, *7*, 050701.
- [48] L. Zhu, H. Yu, H. Zhang, J. Shen, L. Xue, C. Gao, B. Van Der Bruggen, **2015**, *RSC Adv.*, *5*, 73068.
- [49] E. E. Sann, Y. Pan, Z. Gao, S. Zhan, F. Xia, *Sep. Purif. Technol.* **2018**, *206*, 186.
- [50] Y. Ran, Y. He, G. Yang, J. L. H. Johnson, S. H. Yalkowsky, *Chemosphere* **2002**, *48*, 487.
- [51] G. Pandey, C. Rao, *Int. J. Complement Alt. Med.* **2018**, *11*, 355.
- [52] G. Calabrese, G. De Luca, G. Nocito, M. G. Rizzo, S. P. Lombardo, G. Chisari, S. Forte, E. L. Sciuto, S. Conoci, *Int. J. Mol. Sci.* **2021**, *22*, 11783.
- [53] S. Tai, Y. Sun, J. M. Squires, H. Zhang, W. K. Oh, C. Z. Liang, J. Huang, *Prostate* **2011**, *71*, 1668.
- [54] W. Wang, J. I. Epstein, *Am. J. Surg. Pathol.* **2008**, *32*, 65.
- [55] Raphael de Moura Ferraz, L., Gonçalves-Alves, A. E., Souza da Silva-Nascimento, D. D., Silva Ferreira, A., De Albuquerque-Wanderley, V., Rodrigues-Silva, J., Alves-Júnior, S., Araújo Rolim, L., De Souza Pereira, J., Rolim-Neto, P. J., *Sci. Rep.* **2020**, *10*, 16815.
- [56] P. D. Harvey, J. Plé, *J. Inorg. Organomet. Polym.* **2021**, *31*, 2715.
- [57] J. Cadet, J. R. Wagner, *CSH Perspect. Biol.* **2013**, *5*, a012559.
- [58] A. Clausen, T. McClanahan, S. G. Ji, J. H. Weiss, *PLoS One* **2013**, *8*, e83347.
- [59] M. Hoop, C. F. Walde, R. Riccò, F. Mushtaq, A. Terzopoulou, X. Z. Chen, A. J. de Mello, C. J. Doonan, P. Falcáro, B. J. Nelson, J. Puigmartí-Luis, S. Pané, *Appl. Mater. Today* **2018**, *11*, 13.
- [60] Y. S. Ding, H. Wang, J. J. Niu, M. Y. Luo, Y. M. Gou, L. N. Miao, Z. Zou, Y. Cheng, *Int. J. Mol. Sci.* **2016**, *17*, 558.

- [61] L. Wasim, M. Chopra, *Cell. Oncol.* **2018**, *41*, 201.
- [62] S. Shyamsivappan, R. Vivek, A. Saravanan, T. Arasakumar, T. Suresh, S. Athimoolam, P. S. Mohan, *Bioorg. Chem.* **2020**, *97*, 103709.
- [63] M. D. J. Velásquez-Hernández, R. Ricco, F. Carraro, F. T. Limpoco, M. Linares-Moreau, E. Leitner, H. Wilsche, J. Rattenberger, H. Schröttner, P. Frühwirt, E. M. Stadler, G. Gescheidt, H. Amenitsch, C. J. Doonan, P. Falcato, *Cryst. Eng. Comm.* **2019**, *21*, 4538.
- [64] J. Zhuang, C. H. Kuo, L. Y. Chou, D. Y. Liu, E. Weerapana, C. K. Tsung, *ACS Nano* **2014**, *8*, 2812.
- [65] R. Anand, F. Borghi, F. Manoli, I. Manet, V. Agostoni, P. Reschiglian, R. Gref, S. Monti, *J. Phys. Chem. B* **2014**, *118*, 8532.
- [66] A. P. Hill, R. J. Young, *Drug Disc. Today* **2010**, *15*, 648.

Manuscript received: February 19, 2025

Revised manuscript received: April 29, 2025

Version of record online: ■ ■ ■